ORNL/NUREG/TM-181

Creepdown of Zircaloy Fuel Cladding—Initial Tests

D. O. Hobson

Prepared for the U.S. Nuclear Regulatory Commission
Office of Nuclear Regulatory Research
Under Interagency Agreements DOE 40-551-75 and 40-552-75

OAK RIDGE NATIONAL LABORATORY
OPERATED BY UNION CARBIDE CORPORATION · FOR THE DEPARTMENT OF ENERGY

Printed in the United States of America. Available from
National Technical Information Service
U.S. Department of Commerce
5285 Port Royal Road, Springfield, Virginia 22161
Price: Printed Copy $4.50; Microfiche $3.00

This report was prepared as an account of work sponsored by an agency of the United States Government. Neither the United States Government nor any agency thereof, nor any of their employees, contractors, subcontractors, or their employees, makes any warranty, express or implied, nor assumes any legal liability or responsibility for any third party's use or the results of such use of any information, apparatus, product or process disclosed in this report, nor represents that its use by such third party would not infringe privately owned rights.

ORNL/NUREG/TM-181
Distribution
Category NRC-3

Contract No. W-7405-eng-26

METALS AND CERAMICS DIVISION

CREEPDOWN OF ZIRCALOY FUEL CLADDING — INITIAL TESTS

D. O. Hobson

Manuscript Completed — February 10, 1978
Date Published — April 1978

NOTICE: This document contains information of preliminary nature. It is subject to revision or correction and therefore does not represent a final report.

Prepared for the
U.S. Nuclear Regulatory Commission
Office of Nuclear Regulatory Research
Under Interagency Agreements DOE 40-551-75 and 40-552-75

Prepared by the
OAK RIDGE NATIONAL LABORATORY
Oak Ridge, Tennessee 37830
operated by
UNION CARBIDE CORPORATION
for the
DEPARTMENT OF ENERGY

FOREWORD

Previous reports related to this program are listed below:

The Effect of Thermal Transients on the Hardness of Zircaloy Fuel Cladding, ORNL/NUREG/TM-26 (June 1976).

Zircaloy Fuel Cladding Collapse Test Plan, ORNL/NUREG/TM-45 (August 1976).

Quarterly Progress Report on the Creepdown and Collapse of Zircaloy Fuel Cladding Program Sponsored by the NRC Division of Reactor Safety Research for January–March 1976, ORNL/NUREG/TM-51.

Quarterly Progress Report on the Creepdown and Collapse of Zircaloy Fuel Cladding Program Sponsored by the NRC Division of Reactor Safety Research for April–June 1976, ORNL/NUREG/TM-52.

Stress Factors for the Deformation Systems of Zirconium Under Multiaxial Stress, ORNL/NUREG-10 (December 1976).

Interim Report on the Creepdown of Zircaloy Fuel Cladding, ORNL/NUREG/TM-103 (May 1977).

Quarterly Progress Report on the Creepdown and Collapse of Zircaloy Fuel Cladding for July 1976–March 1977, ORNL/NUREG/TM-125.

Design and Safety Report for Hobbie Capsules (A Series of Zircaloy Creepdown Irradiation Tests), ORNL/NUREG/TM-167 (December 1977).

CONTENTS

FOREWORD iii

ABSTRACT 1

INTRODUCTION 1

Applications to Reactor Safety 2

Concepts of Creepdown Testing 3

Geometrical 4

Textural 4

APPLICABLE PRIOR WORK 5

EXPERIMENTAL PROCEDURE 7

EXPERIMENTAL RESULTS AND DISCUSSION 9

Test Data 10

Data Analysis 11

Graphical and analogue modeling 19

Mathematical modeling 28

FUTURE WORK 32

Short-Term Tests 32

Long-Term Tests 33

CONCLUSIONS 33

ACKNOWLEDGMENTS 34

CREEPDOWN OF ZIRCALOY FUEL CLADDING — INITIAL TESTS

D. O. Hobson

ABSTRACT

This report describes the initial creepdown tests of Zircaloy Fuel Cladding in which the surface displacements of the specimens have been measured as a function of time. Such measurements were made with a high accuracy, high precision eddy-current device capable of operation at elevated temperatures and pressures.

Tests were conducted at 371°C (700°F) and external pressures of 14.5 to 17.2 MPa (2100 to 2500 psig) on specimens of reactor grade Zircaloy-4 fuel cladding in the unirradiated, stress relieved condition. Data are reported in several forms — as individual radial displacements of the cladding surface with time; as average diameter and ovality changes with time; in sequential photographs of analogue models; and with a preliminary discussion of mathematically modeled surfaces.

It is concluded that the creepdown phenomenon, although complicated to test and describe, may not be as difficult to understand as previously thought. Further testing will refine our present knowledge of cladding behavior relative to strain behavior under creep conditions.

INTRODUCTION

Presentday light-water power reactors are fueled with UO_2 pellets contained in Zircaloy-4 tubes. These tubes are combined into fuel bundles that typically contain 220 to 290 tubes, of which a large fraction will contain the UO_2 pellets. The remainder consist of instrumentation tubes, control rods, etc. Hundreds of these fuel bundles make up the core of the power reactor.

Under normal reactor operating conditions the Zircaloy fuel cladding tubes are subjected to external hydrostatic pressure from the coolant water. This pressure is typically about 16 MPa (2300 psig) for a pressurized water reactor (PWR). This external pressure must be supported by the cladding with the aid of any internal prepressurization and the

buildup of fission products during reactor operation. The load supported by the cladding can, at the operating temperature of that cladding, cause a slow deformation of the cladding onto the fuel pellets. This deformation, for which the descriptive term "creepdown" has been coined, is of great importance in the long-term behavior of fuel rods in a power reactor.

Applications to Reactor Safety

Nuclear reactor safety regulations require that reactor designs be capable of meeting certain safety criteria. Such criteria include a specified "maximum credible accident" — a double-ended guillotine break of the largest coolant water pipe to the reactor pressure vessel — the hypothetical loss-of-coolant accident (LOCA). Reactor vendors must show that the emergency core cooling system (ECCS) of the reactor can perform adequately and meet the applicable criteria.

The present study is not directed at an accident situation *per se*, in the sense that there are no specific criteria for creepdown as related to hypothetical accidents. This study is of major importance however, because it quantifies certain aspects of cladding behavior, behavior that can directly affect the way in which the ECCS handles accidents.

During the first few seconds of an LOCA, in which the contents of the pressure vessel are flashing to steam and venting through the pipe break, the rate of heat transfer from the fuel pellets to the exiting coolant largely determines the thermal behavior of the core. Significant amounts of heat are contained in the fuel pellets, and this heat must be dissipated to the coolant during blowdown.

In normal operation heat is transferred by conduction through the cooler outer layers of the UO_2, the pellet-to-cladding gas gap, the cladding, and into the coolant. The pellet-to-cladding gas gap typically measures 0.1 to 0.13 mm (0.004 to 0.005 in.) radially in a new fuel rod. With time, this gap will change until the cladding can actually be in close contact with the pellet as a result of creepdown and pellet swelling. This varying heat transfer gap is of great importance to fuel rod designers and modelers of fuel element behavior.

In addition to the heat-transfer aspects of gap thickness, there is another phenomenon of interest to analysts of fuel rod behavior. As soon as the fuel cladding is in close contact with the fuel pellets, mechanical interaction can occur. This pellet-cladding mechanical interaction (PCMI) can lead to time-independent strains in the cladding. An idea of the importance of this is given by a quote from the introduction to a recent report by Bohn of INEL:[1]

> "The analysis of stress and strain in the cladding of nuclear reactor fuel rods is of paramount importance in predicting rod failure under different normal and off-normal operating conditions. The mechanical behavior of the fuel rod cladding and the fuel pellets which are contained within the cladding is inseparably coupled with the thermal-hydraulic response of the fuel rods and the surrounding coolant. Without simultaneously considering all the mutual interactions which can occur, it is not possible to realistically analyze the true behavior of the fuel rods."

The FRACAS subcode deals primarily with the effects of fuel pellet swelling and thermal expansion on the gap closure between the pellets and the cladding. However, the statement quoted above also applies to creepdown effects.

Concepts of Creepdown Testing

The experimental determination of the rate at which the Zircaloy cladding deforms under external pressure is a difficult problem — one that has not been successfully studied in the past. Creep data from uniaxial tensile creep tests and from internally pressurized tubes occasionally have substituted for the correct-stress-state data generated by the externally-pressurized tests. It is very important to understand the limitations of the data obtained by the various testing methods, especially because the data are *not* generally interchangeable in their applicability for modeling the mechanical behavior of Zircaloy.

---

[1]M. P. Bohn, *FRACAS, A Subcode for the Analysis of Fuel Pellet — Cladding Mechanical Interaction,* TREE-NUREG-1028 (April 1977).

Why should creep behavior differ between internally pressurized and externally pressurized closed-end tubes? Two general concepts address the question — geometrical and textural.

Geometrical

An internally pressurized tube with closed ends is in a biaxial tensile stress state with a 2/1 ratio of tangential or hoop stress to axial stress. As creep occurs both components of the biaxial stress state remain tensile and the tubular specimen should remain relatively stable until wall thinning and rupture occur.

An externally pressurized tube with closed ends is also in a 2/1 biaxial stress state. Both stresses are compressive in this case, however, and the specimen can *never* be stable. Generally, any initial ovality in the tubing cross section will increase, and the rate of deformation will accelerate. In addition, the stress state will not remain constant as deformation proceeds. Rather, bending will produce in the tubing wall additional tensile and compressive stress components that will modify the initial stress state. Such behavior is much more complex to analyze than that caused by internal pressurization.

Textural

Several literature sources[2,3] have stated that (1) texture effects on strength can persist at temperatures exceeding 400°C (752°F), and (2) mechanisms proposed for in-reactor creep in Zircaloy at stresses above 100 MPa (14.5 ksi) suggest that a strength differential effect proportional to that observed in short-term yield deformation may occur in in-reactor creep as well.

Textures that occur in typical Zircaloy fuel cladding — basal poles distributed about points ±30° from the radial direction toward the tangential — can strongly affect the yield behavior of that material.

---

[2]J. A. Jensen, thesis cited by G. E. Lucas and A. L. Bement, "The Effect of a Zirconium Strength Differential on Cladding Collapse Predictions." *J. Nucl. Mater.* 55: 246–52 (1975).

[3]F. A. Nichols, paper cited by G. E. Lucas and A. L. Bement, "The Effect of a Zirconium Strength Differential on Cladding Collapse Predictions," *J. Nucl. Mater.* 55: 246–52 (1975).

Zircaloy resists deformation in compression along the basal pole more than it does from stress away from the basal pole. One would infer, therefore, that an internally pressurized tube with its 2/1 biaxial tensile stress state would exhibit greater strength than an externally pressurized tube. The rationale is that strain in the internally pressurized tube typically requires wall thinning — a deformation that is opposed by the texture, for the reason given above.

The question now arises whether texture influences creep behavior as it does yield strength. Causey[4] has shown a relationship between irradiated yield strength and creep rate for several zirconium-base alloys including Zircaloy-2 and -4. Most of the differences in yield strength appear to be related to both heat treatment and cold work rather than to texture, so that the effect of texture is not clear.

APPLICABLE PRIOR WORK

The applicability of any experimental data to the problem of cladding creepdown must be tested against the following criteria:

1. are the data continuous with time, at least to a close approximation;
2. can cladding surface displacements be separated from bowing effects;
3. are the data both highly precise and highly accurate;
4. is the proper stress state used;
5. can the cladding shape be discerned as a function of time;
6. is the pellet-cladding gap modeled adequately;
7. are in-reactor data available that meet the preceding criteria?

The above criteria form a very restrictive set against which any experimental data are to be judged. Yet these criteria are necessary if the goal of understanding cladding movement under normal or near-normal reactor operating conditions is to be achieved successfully. As of this writing, no open literature data successfully meet all the criteria. However, the present work does meet the first six, and with the initiation of the in-reactor testing in 1978 all seven criteria will be met.

---

[4]A. R. Causey, "In-Reactor Creep of Zircaloy-2, Zircaloy-4 and Zr—1.15 wt % Cr—0.1 wt % Fe at 568 K Derived from their Stress-Relaxation Behavior," *J. Nucl. Mater.* 54: 64—72 (1974).

Some explanation of the rather critical statement concerning inapplicability is appropriate. Criterion 2 gives an example of the nuances of the creepdown problem. Data are becoming available in the literature from measurements of diametral strains with time. For instance, data recently reported from Halden[5] appear to satisfy several of the above criteria, including those of high precision, correct stress state, cladding shape, and having been taken in-reactor. The strains that are reported (as diametral strains) are measured in a radial direction, but the probe is positioned and referenced by two fixed arms that rest against the cladding surface 120° from the probe. As far as the author can tell, such a setup cannot distinguish between bowing and radial surface displacements and, if the reference arms are indeed spaced 120° from the probe, a true diametral measurement is not obtainable. The advantage of the Halden experiments over the present experiments rests on their ability to measure over a large area of the fuel rod surface. The present experiments are limited to 20 selected points on a tube within a 51-mm (2-in.) length.

Clevenger[6] of Babcock and Wilcox recently reported diametral measurements made by a spiral scanning technique. This method is unique in that it measures with high precision both the magnitude and circumferential position of the ovality in the cladding over its full length. The criteria listed earlier indicate two disadvantages in this technique, however: the discontinuity of the measurements and the lack of separate radial surface displacement measurements.

It can be assumed that reactor vendors maintain proprietary creepdown data. Unfortunately such information is not available for comparison with the open literature data.

---

[5]K. D. Knudsen, OECD Halden Reactor Project, "In-Pile Measurements of Fuel Rod Deformation," presented at the USNRC Fifth Water Reactor Safety Research Information Meeting, Washington, D. C., November 7–11, 1977.

[6]G. Clevenger, informal talk given at the USNRC Fifth Water Reactor Safety Research Information Meeting, Washington, D. C., November 7–11, 1977.

see p. 19

EXPERIMENTAL PROCEDURE

Many aspects of the experimental procedure used in this study have been reported previously[7–9] and will not be given in detail in this report. However, an overview will describe the procedures used.

Tubular specimens 152 mm (6 in.) long were cut from the standard lot of Zircaloy cladding supplied by Sandvik Special Metals Corp. and described by Chapman.[10] Care was taken to choose tubes with as little variation in wall thickness and diameter as possible. Zircaloy end plugs were welded into the ends of the tubes, as previously described. An atmospheric vent tube was attached to the stem of one of the end plugs. Contained within each specimen was a stainless steel mandrel, machined to provide the desired simulated pellet-to-cladding gap: the radial distance between the mandrel and specimen wall was generally 0.10 to 0.13 mm (0.004 to 0.005 in.). In one instance a simulated pellet-to-pellet gap of 20 mm (0.80 in.) was used to show how the specimen wall deforms into the gap as a function of time.

The specimen was centered in a thick-walled aluminum cylinder that contained the eddy-current coil-probe assemblies — 20 measuring assemblies, three reference lift-off coils, and one null balance coil. The latter four coils constantly check the accuracy of the data. The cylinder assembly is shown in Fig. 1. Each coil is grounded under the holddown screw adjacent to the coil, and the "hot" leads are taken out of the autoclave in stainless steel sheaths. Because of the high frequency involved (2 MHz), grounding and shielding are of great importance for maintaining stable signals from the coils to the instrument. Almost a year was spent developing and refining the electrical hookup procedures before reliable data were obtained. The measuring system now operates in a stable manner, with both high accuracy and high precision.

---

[7] D. O. Hobson, *Zircaloy Fuel Cladding Collapse Test Plan*, ORNL/NUREG/TM-45 (August 1976).

[8] D. O. Hobson and C. V. Dodd, *Interim Report on the Creepdown of Zircaloy Fuel Cladding*, ORNL/NUREG/TM-103 (May 1977).

[9] D. O. Hobson, *Quarterly Progress Report on the Creepdown and Collapse of Zircaloy Fuel Cladding for July 1976–March 1977*, ORNL/NUREG/TM-125 (July 1977).

[10] R. H. Chapman (Compiler), *Characterization of Zircaloy-4 Tubing Procured for Fuel Cladding Research Programs*, ORNL/NUREG/TM-29 (July 1976).

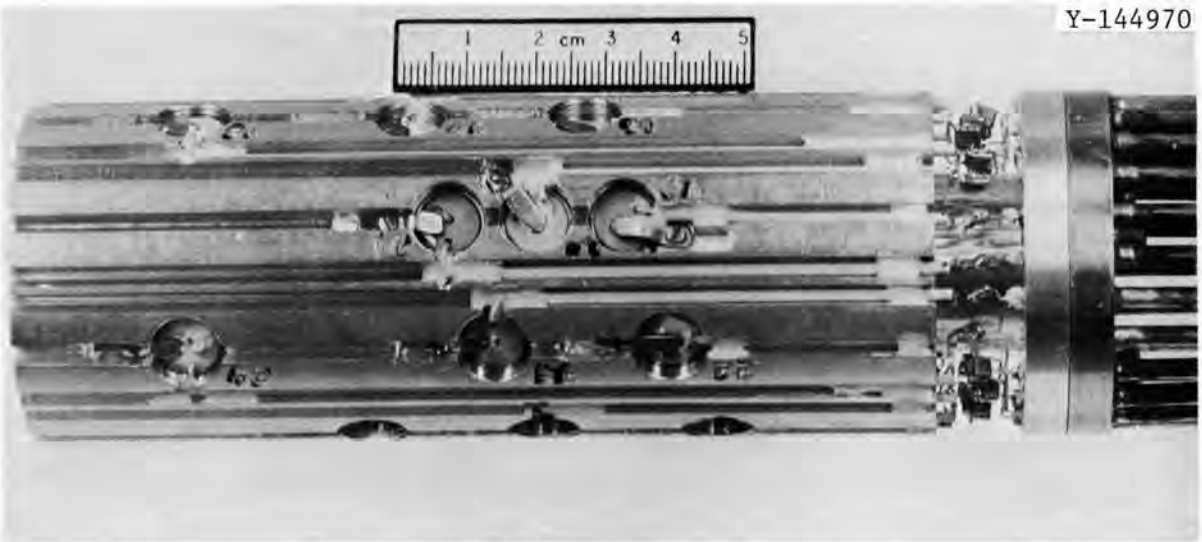

Fig. 1. Eddy-Current Coil Block. Helical array of working coils is shown in center and two of the reference lift-off coils on left. Shielded cables are shown on the right.

The microcomputer-controlled data acquisition instrument monitors the signals from the 20 working probes, compares the signals relative to the null balance coil, and converts them to direct displacement readings which are printed out and recorded on magnetic tape for further processing. Data were normally recorded at 2-hr intervals. In the longer tests, 10,000 to 13,000 individual surface displacements were read. Differences in displacements as small as 1 μm (0.00004 in.) were measured over the 2-hr data acquisition intervals.

The tests were conducted within a heavy-walled steel autoclave, which was externally heated by a resistance-heated furnace. This setup provided a high-heat-capacity system with virtually no temperature variation within the autoclave. Autoclave pressure, the external helium pressure on the specimen, was supplied by a gas booster pump. The system was sufficiently gastight that only periodic pumping was needed to restore the correct pressure. Typical losses were 0.345 MPa (50 psig) in approximately 48 hr at a pressure level of 15.9 MPa (2300 psig).

Data were recorded on magnetic tape and then stored in a PDP-10 computer for subsequent processing. The displacement of each probe could then be plotted as a function of time or else the data could be operated on to give average diameter change, maximum ovality, or any other functional relationship desired.

EXPERIMENTAL RESULTS AND DISCUSSION

The six tests run to date are listed in Table 1. The first three tests were used to check out the experimental equipment and utilized annealed tubing specimens from the earlier collapse portion of this study. The last three tests were made with as-received, stress-relieved tubing and were run for longer times. These latter tests are part of a series of tests to be run at progressively lower pressures in an attempt to provide a data base from which the creepdown behavior of real reactor fuel cladding can be extrapolated. In a new fuel loading, the cladding is probably subjected to a differential pressure of from 10 to 12 MPa (1450–1750 psig) due to prepressurization. The buildup of fission product gas lowers this differential. A goal of this study is eventually to perform long-time experiments at differential pressures as low as 13.1 MPa (1900 psig).

Table 1. Creepdown Test Descriptions
[all at 371°C (700°F)]

Test	Pressure		Time (hr)
	(MPa)	(psig)	
458-1050-4[a]	17.24	2500	250
254-1050-8[a]	15.86	2300	350
254-1050-4[a,b]	15.86		200
269-8	15.86		950
269-27[c]	15.86		1270
269-4	14.48	2100	1000

[a]Specimen tubes given low temperature (565°C) anneal. All others in as-received, stress-relieved condition.

[b]Specimen had 0.125 mm (0.005 in.) initial ovality.

[c]Specimen had a 20.3 mm (0.8 in.) simulated pellet-to-pellet gap in the mandrel.

In general, the eddy-current measuring equipment performed exceptionally well throughout the long-term tests. A single coil-probe

assembly was lost in test 269-8 and another in test 269-27, but data acquisition remained stable. Incidentally, only three coils have had to be replaced during the 4000 hr at testing to date. Breakage of the thin aluminum leads from the coils to the shielded leads necessitated each replacement.

Test Data

Data from tests 269-8, 269-27, and 269-4 were found to have discontinuities in the displacements. An example of this is shown in Fig. 2 for test 269-4, with curves for probes 13 through 17. Vertical discontinuities occurred at 20, 522, and 744 hr. The data from the other 15 working coils showed similar displacements. Analysis of the data showed the displacements to be linear with output voltage from the analogue-to-digital converter in the eddy-current instrument. We attribute the displacements to the random addition or withdrawal of a grounding path among the multiple paths provided by the conductor sheaths. Two adjacent sheaths could make contact, or a sheath could touch the autoclave wall during the test. The range of the data acquired by the 20 coils, however, was small enough that a linear correction based on lift-off could be used to correct the data. The correction operation is analogous to the correction that is routinely applied to more prosaic tensile creep tests after the creep frame has been kicked accidentally — the displaced data are simply translated vertically until the curves match.

On the following pages the corrected curves are shown for the individual coil-probe assemblies for the three long-term tests. *Note that the "change in lift-off" scale multiplies values by 100, for example, 10.0 is equivalent to 0.10 mm (0.0039 in.).* Also included are the curves for the reference lift-off coils — Numbers 6, 12, and 18. These latter curves are uncorrected, so that the data discontinuities are easily seen. It should be emphasized that only Coil 6 was at a reference lift-off value near the operating range of the 20 working coils. Coils 12 and 18 were at much greater lift-off distances and were more sensitive to line voltage and room temperature fluctuations. (Note the 24-hr periodicity of the ouput from Coil 18). As long as Coil 6 showed little or no variation there was good assurance that the test data were accurate as well as precise.

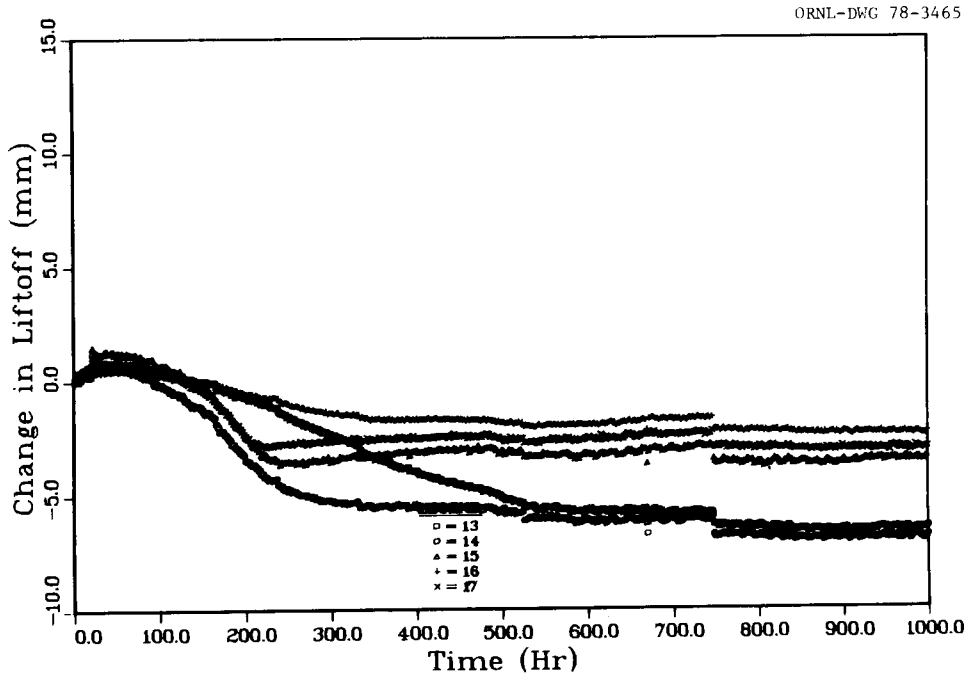

Fig. 2. Raw Data from Several Probes in Test 269-4. Notice discontinuities at 22, 522, and 744 hr. "Change in lift-off" scale has been multiplied by 100, i.e. 10.0 is equivalent to 0.10 mm (0.0039 in.).

Figures 3 through 7 illustrate the data for Test 269-8. Note that data for Coil 7 indicate failure of that coil. Figures 8 through 12 illustrate the data for Test 269-27. Data for Coil 4 are missing because of coil failure. Finally, data for Test 269-4 are shown in Figs. 13 through 17.

Data Analysis

A number of mathematical operations can be performed on the mass of accumulated data. Data analysis must be predicated on what is required to describe the creepdown phenomenon. A required analysis is to clearly define the surface displacements that have taken place during the test. Obviously the data have been acquired under a rather rigid geometrical restriction — 20 probes have measured the radial surface displacements of 20 points over a 50.8-mm (2-in.) length of the specimen. The translation of those data into a knowledge of surface displacement rate, of creep rate, of pellet-to-cladding contact time, or of any other pertinent rate-related quantity is complex.

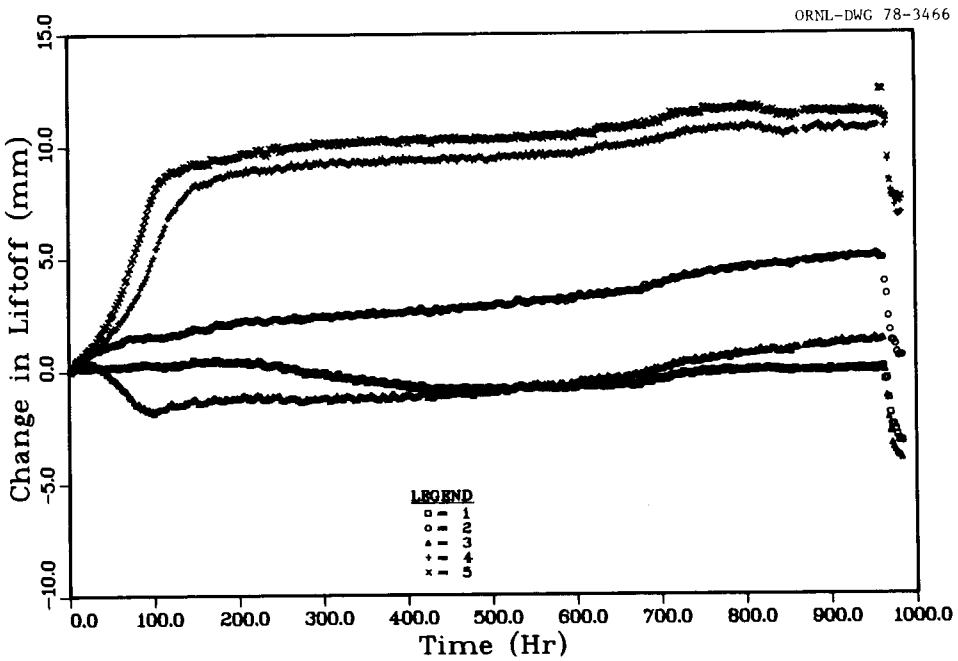

Fig. 3. Corrected Data from Probes 1 through 5, Test 269-8. Points after approximately 960 hr taken during cooldown and depressurization.

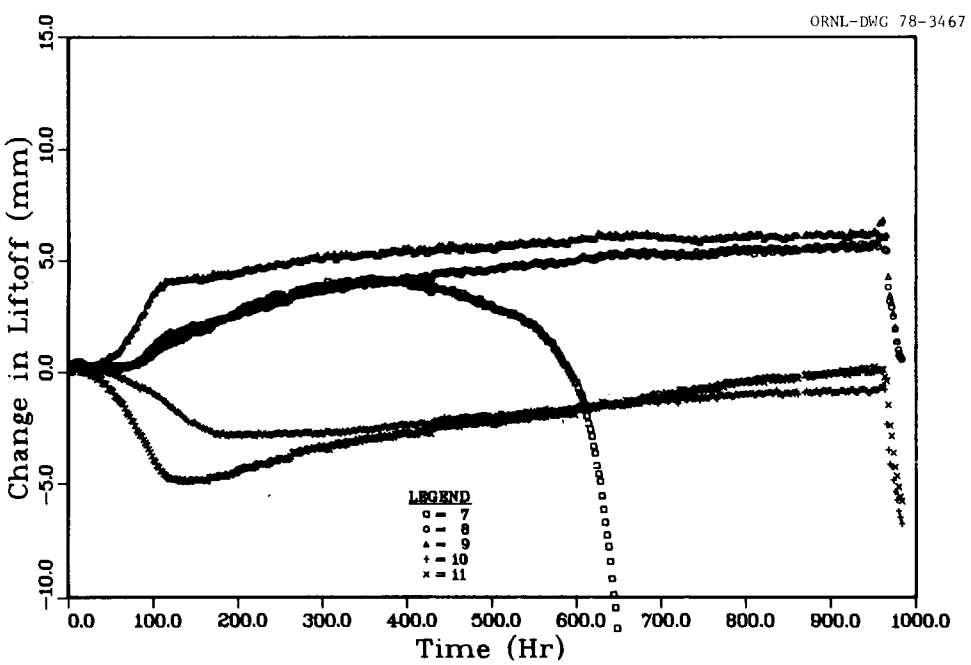

Fig. 4. Corrected Data from Probes 7 through 11, Test 269-8. Coil 7 began to fail at approximately 350 hr.

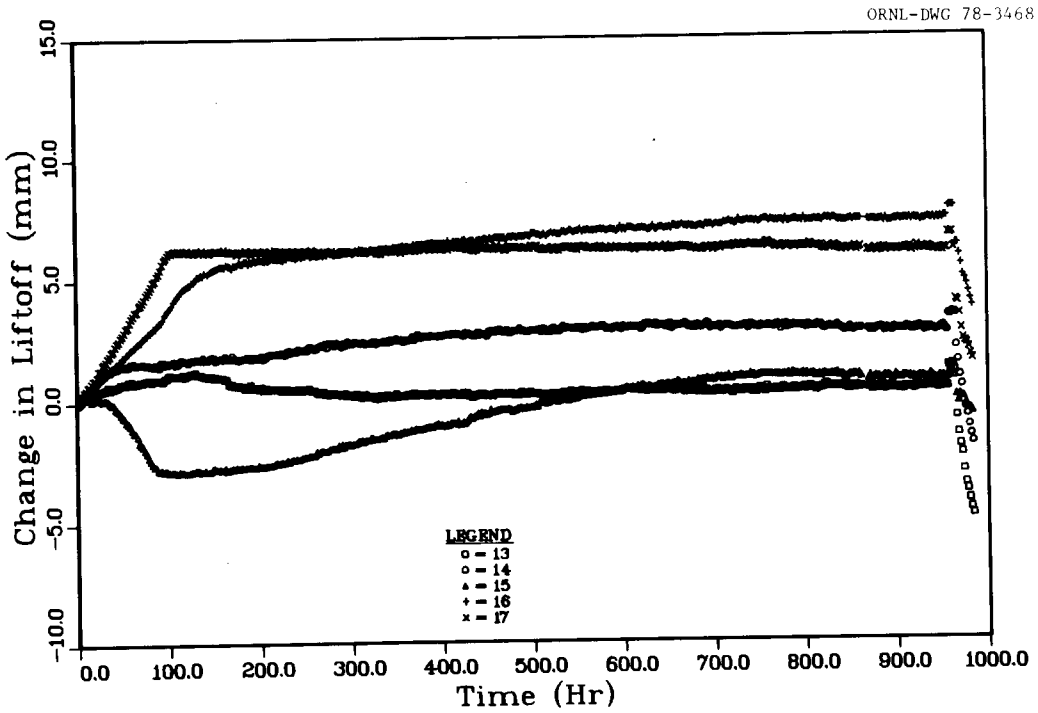

Fig. 5. Corrected data from Probes 13 through 17, Test 269-8.

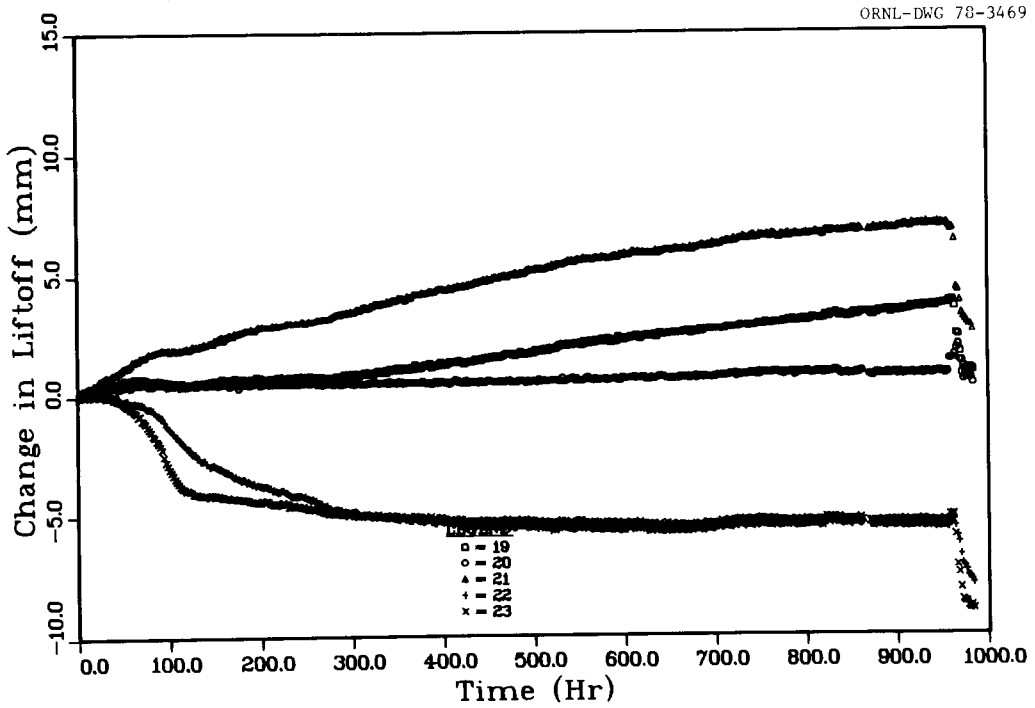

Fig. 6. Corrected Data from Probes 19 through 23, Test 269-8.

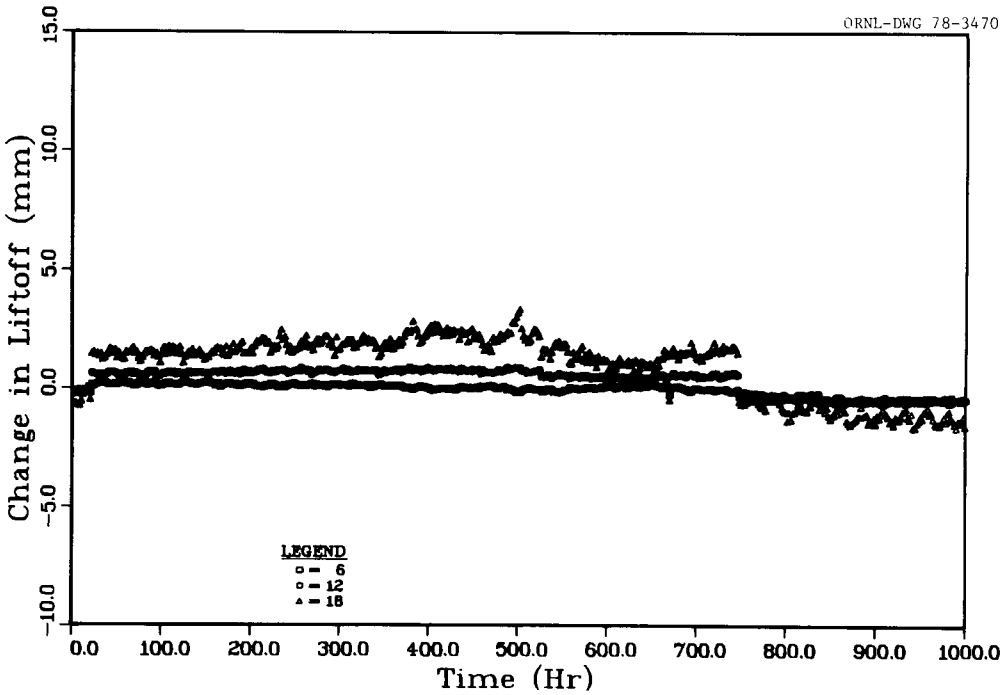

Fig. 7. Uncorrected Data from Reference Lift-Off Coils 6, 12, and 18. Constant values near zero for coil 6 indicates that Test 269-8 remained in good calibration and that the data were of high accuracy as well as high precision.

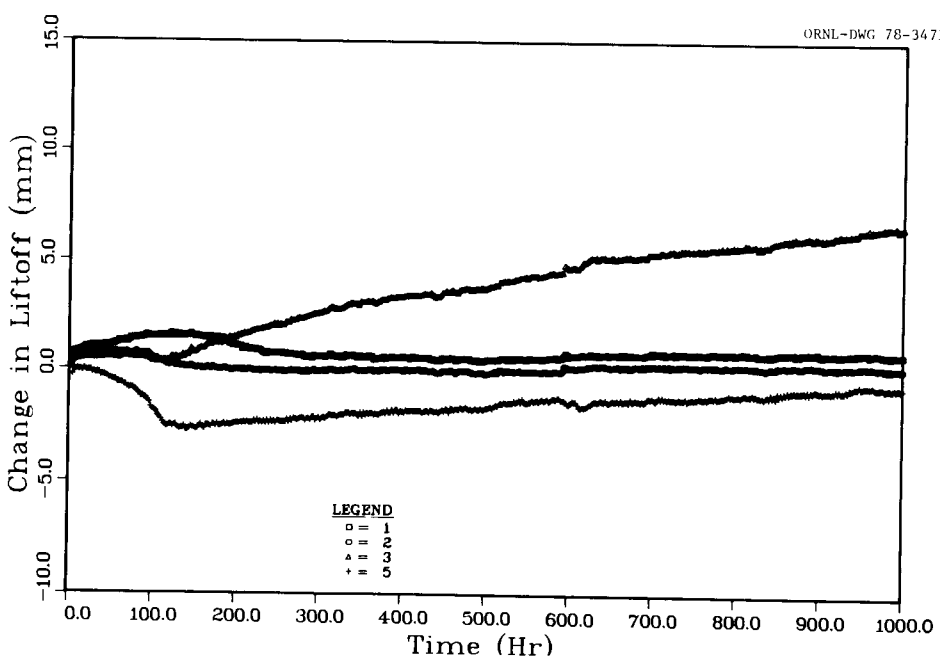

Fig. 8. Corrected Data for Probes 1, 2, 3, and 5 of Test 269-27. Coil 4 failed during the test and is not shown.

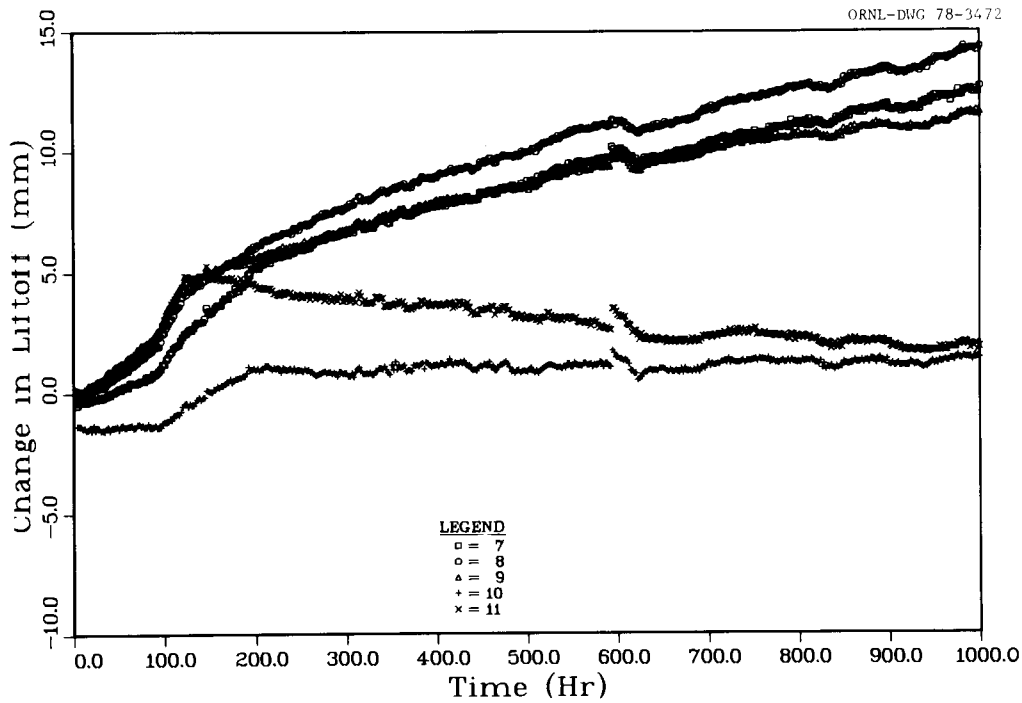

Fig. 9. Corrected Data for Probes 7 through 11 of Test 269-27. The perturbation in the data at approximately 590 hr was coincidental with the loss of coil 4. No correction was applied to it.

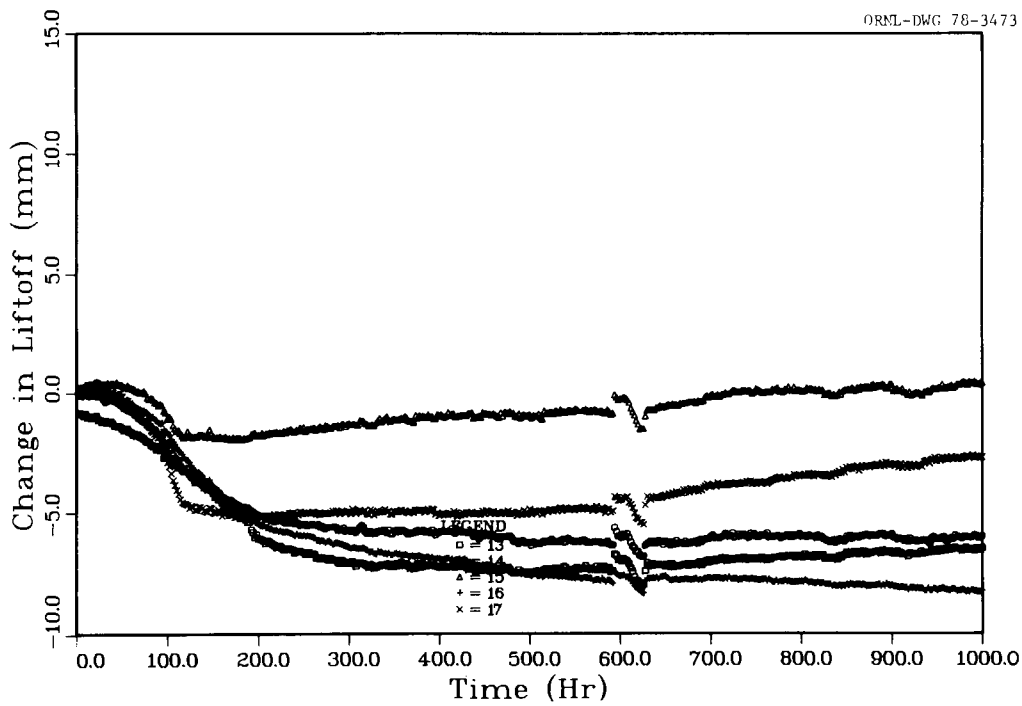

Fig. 10. Corrected Data for Probes 13 through 17 of Test 269-27.

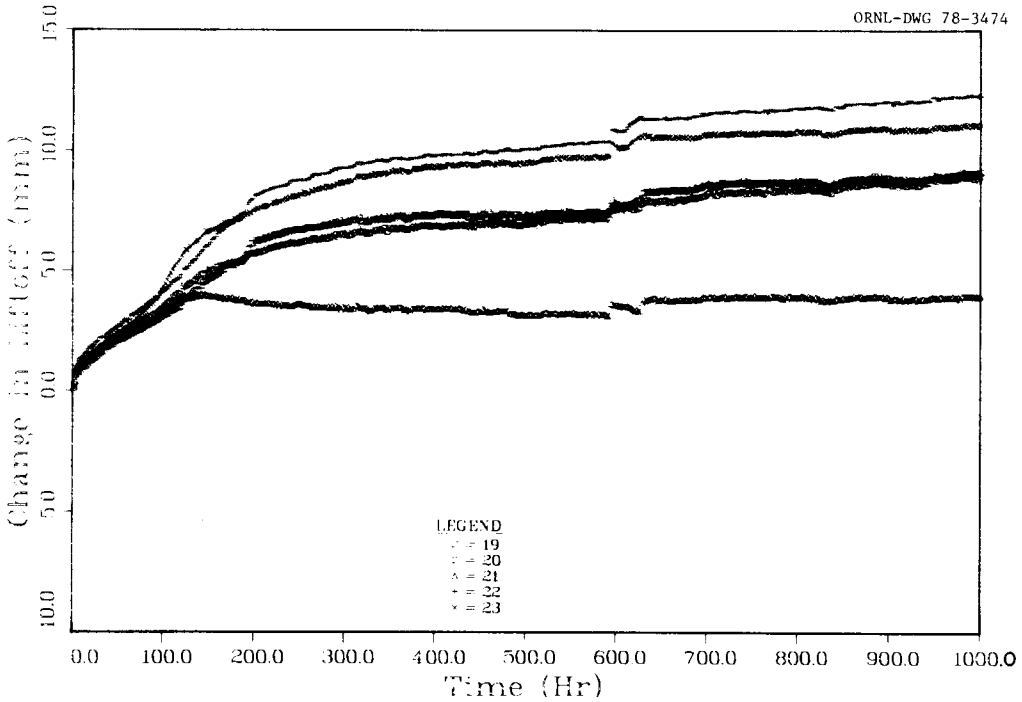

Fig. 11. Corrected Data for Probes 19 through 23 of Test 269-27.

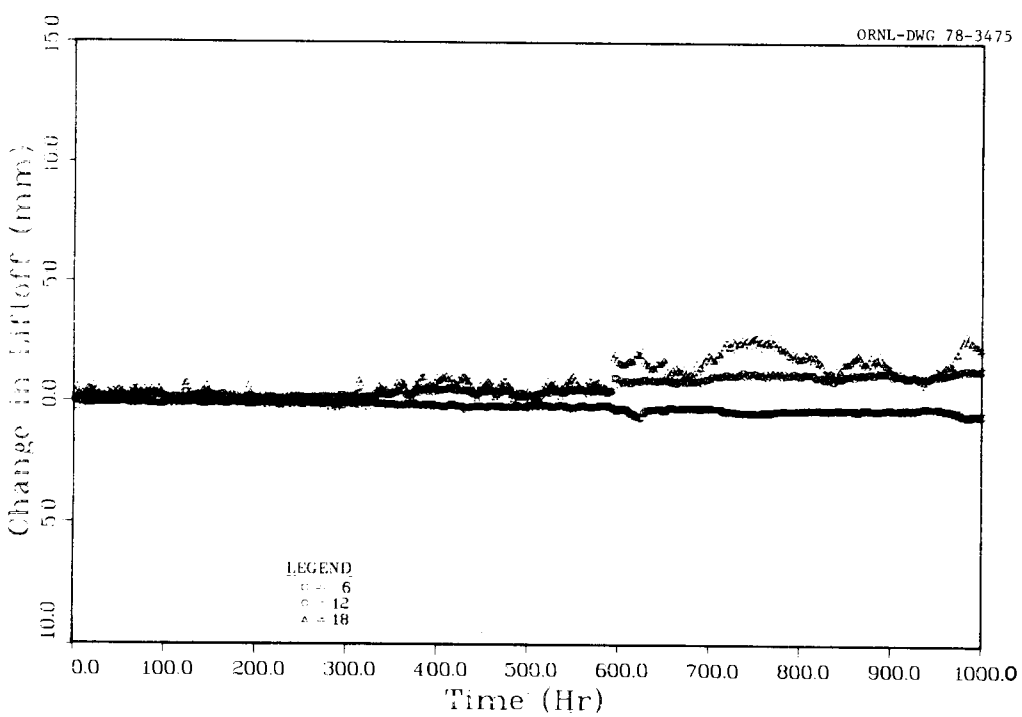

Fig. 12. Uncorrected Data from Reference Lift-Off Coils 6, 12, and 18 for Test 269-27.

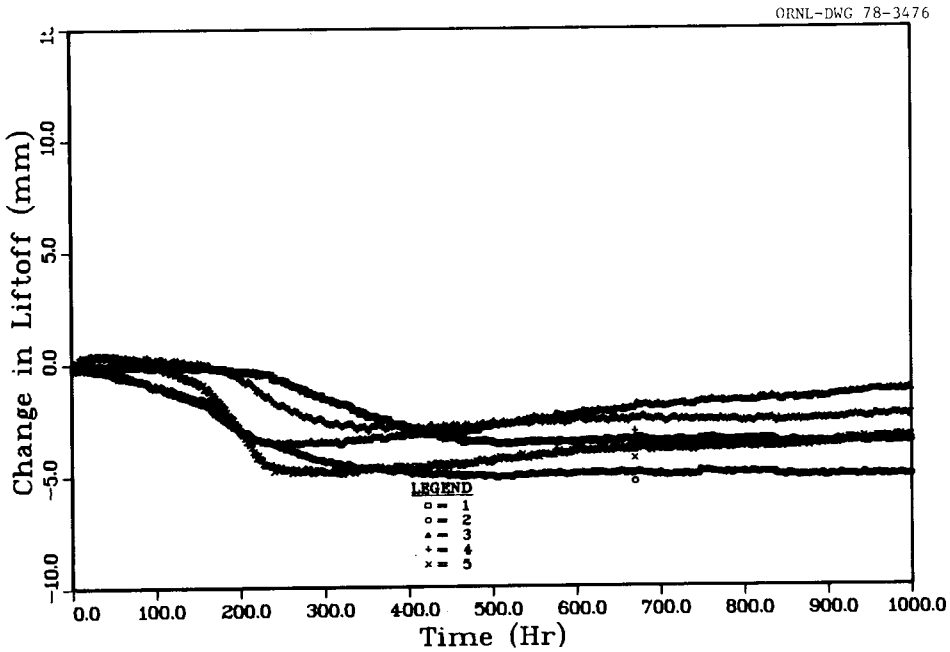

Fig. 13. Corrected Data from Probes 1 through 5 for Test 269-4.

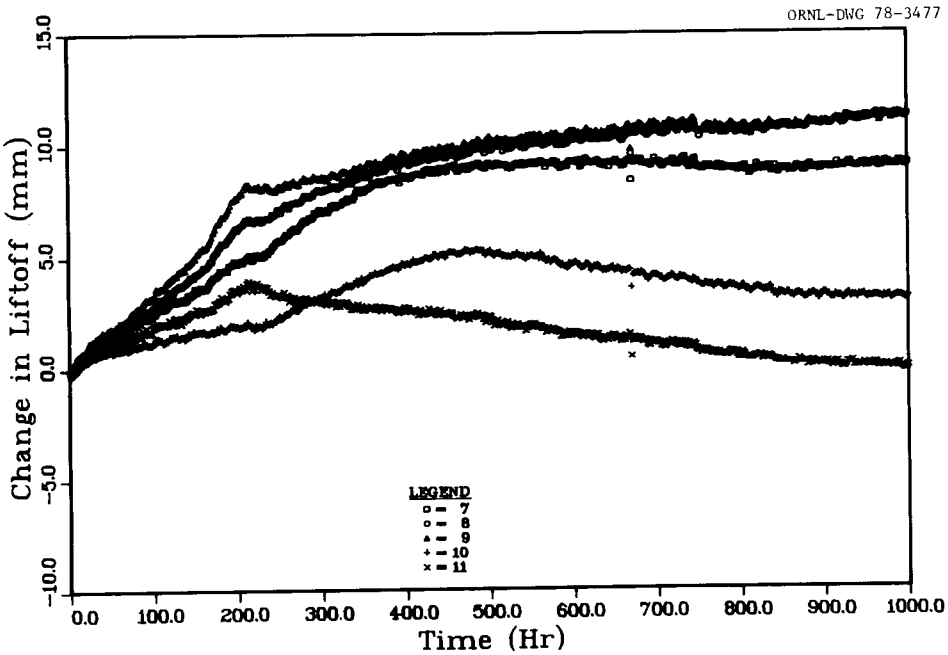

Fig. 14. Corrected Data from Probes 7 through 11 for Test 269-4.

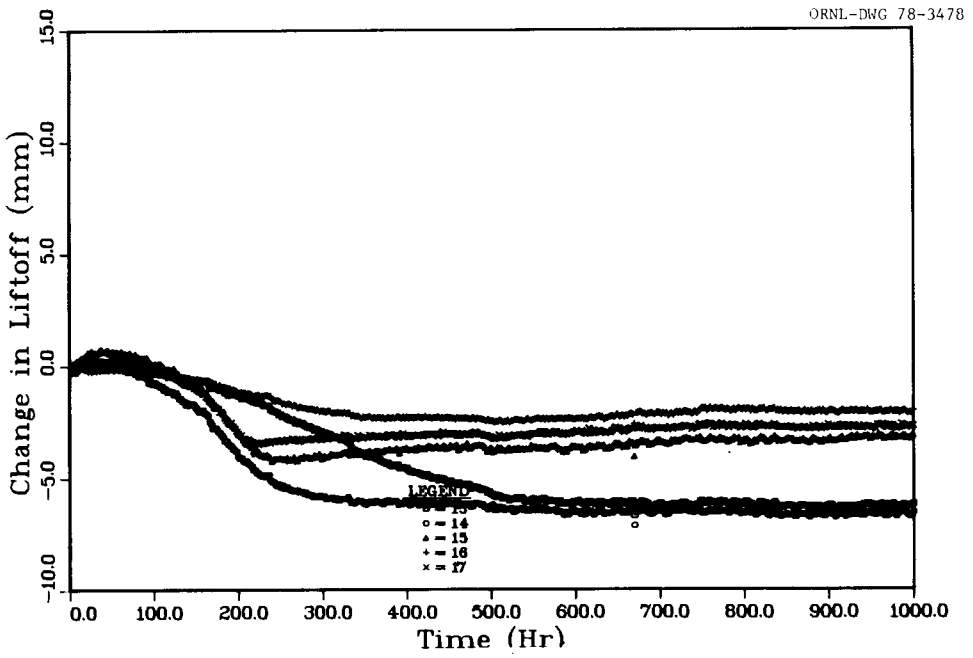

Fig. 15. Corrected Data from Probes 13 through 17 for Test 269-4.

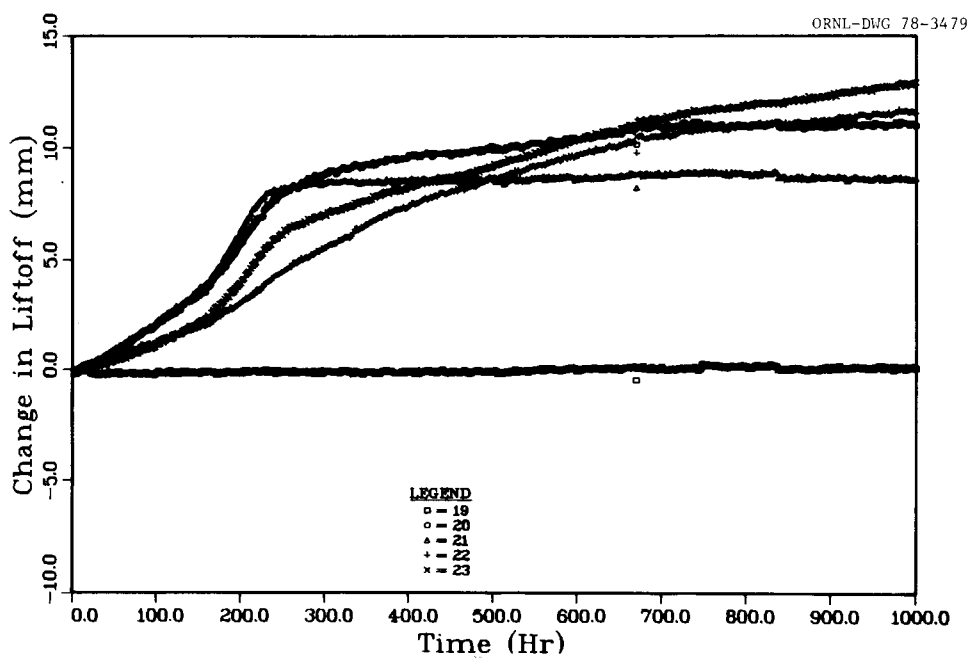

Fig. 16. Corrected Data from Probes 19 through 23 for Test 269-4.

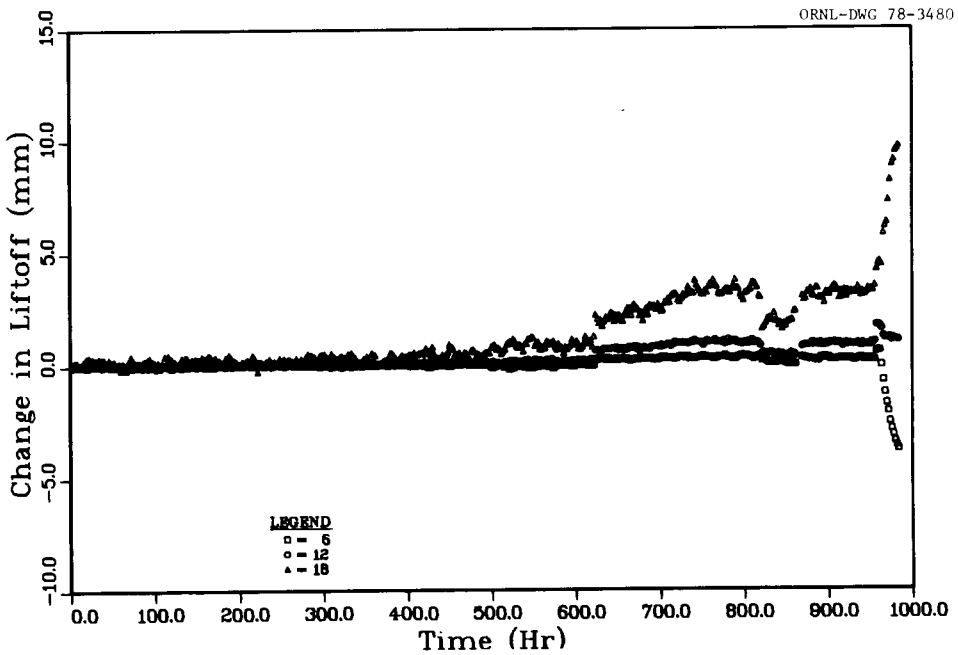

Fig. 17. Uncorrected Data from Reference Lift-Off Coils 6, 12, and 18 for Test 269-4.

Graphical and analogue modeling

Perhaps the easiest task is to show pictorially the step-by-step process of creepdown for the three long-term tests. This has been accomplished with two mechanical models. Figures 18 and 19 show these models. The model depicted in Fig. 18 is a direct analogue of the cylindircal coordinates of the probe geometry. The small rubber O-rings represent the surface position and the metal rods represent the directions along which the probes can move. The latter figure represents a more useful analogue in which the cylindrical "surface" of the specimen has been "unrolled" into a flat plane and the specimen radii are now represented by metal rods normal to that surface. The periodicity of the surface displacements is easily seen.

The changes in surface displacement with time can be seen in the series of small photographs printed in the margins of this report. If the body of this document is flexed and the page edges are released sequentially, the creepdown can be seen in a progression of positions. Successive photographs represent the displacements after 100-hr intervals of elapsed test time. The test identification, the starting point, and the sequence directions are given in Table 2.

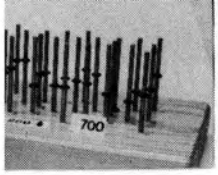

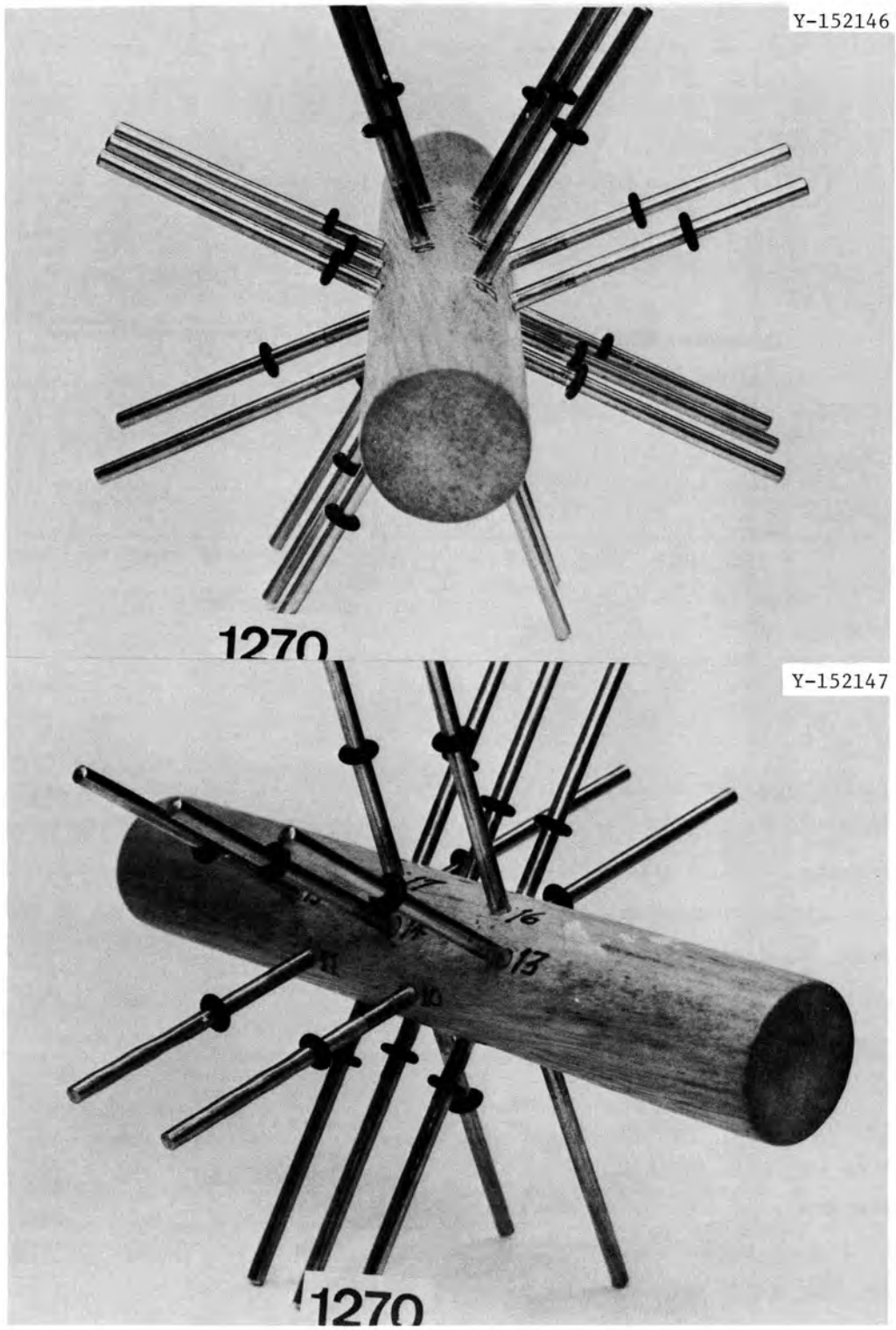

Fig. 18. Cylindrical Analogue of the Surface Displacement of Test 269-27 after 1270 hr. The rubber O-rings represent the radial positions of the surface, and the metal rods represent the axial and circumferential positions of the probes. Reduced 13.5%.

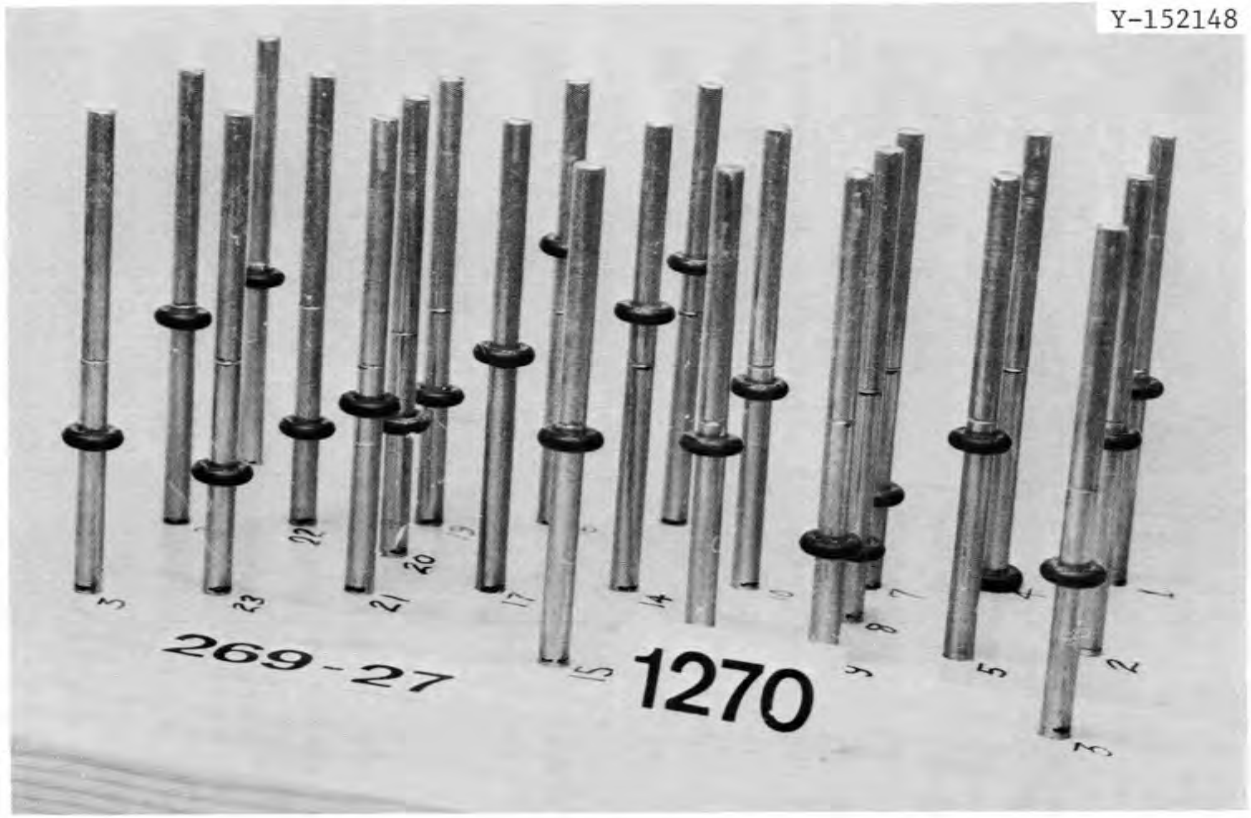

Fig. 19. Flat Analogue of the Surface Displacements of Test 269-27 after 1270 hr. The rubber O-rings represent the radial positions of the surface, and positions of the metal rods represent the axial (front to back) and circumferential (left to right in figure) positions of the probes. The scribed marks at the midpoint of each rod represent the zero-displacement positions of the probes.

Table 2. Border Photograph Identification and Instructions

Test Number	Starting Page Number	Corner Position	"Flip" Direction[a]
269-4	13	Bottom Right	Forward
269-27	7	Upper Right	Forward
269-8	32	Upper Left	Reverse

[a]Forward indicates a progression toward increasing page numbers. Reverse indicates a progression toward decreasing page numbers.

It would be expected from the curves in Figs. 3 through 17 that a large amount of surface movement takes place during the first few hundred hours of testing. This is confirmed in the border sequences, wherein the amplitude of the periodicity of the surfaces first increases rapidly and then increases at slower and slower rates. It should be pointed out that the periodicity tends to occur as two ridges and two valleys — the equivalent of the tendency toward ovalization in the actual specimen.

Test 269-27 is of particular interest because of the simulated pellet-to-pellet gap. Eight of the twenty probes were located within the 20.3-mm (0.8-in.) gap length, and two of these showed definite penetration into the gap. The indicator for Probe 8 (in the middle of the third row from the right) can be seen to drop below its neighbors. The total measured surface diplacement from Probe 8 was 0.162 mm (0.0064 in.). Probe 20, diametrically opposite Number 8, showed a surface displacement of 0.094 mm (0.0037 in.). Since the total diametral gap between the specimen tube and the mandrel was 0.20 mm (0.008 in.), this represents a diametral difference of 0.053 mm (0.0020 in.) or an average radial penetration into the pellet-to-pellet gap of 0.026 mm (0.0010 in.).

In addition to the analyses of surface shape and rate of shape change, examination of the average diameter of the specimens as a function of time is important. The maximum ovality of a specimen increases rapidly with time until the mandrel and cladding contact. From that point the maximum ovality increases quite slowly, if at all. The average diameter, on the other hand, decreases smoothly with time, showing only a small inflection

when the mandrel is contacted. Figures 20 and 21 illustrate these patterns of change in maximum ovality and average diameter, respectively, for specimen 269-4. The two effects are largely decoupled because a diameter decrease is accomodated by wall thickening and/or length increase, whereas ovalization is accomodated by a combination of tensile and compressive strains in the circumferential direction of the specimen.

The three long-term specimens were sectioned through their axial centerlines and through points approximately 22 mm (0.9 in.) from those axial center points. These six surfaces were polished, and a high-accuracy tool-makers microscope equipped with a digital readout[11] was used to measure specimen radii (inner and outer surfaces). These measurements provided inside and outside diameters and wall thicknesses. The wall thickness variations are of particular interest and are shown in Fig. 22 as a function of specimen circumference. The axial centerline sections were unsupported by the mandrel: specimen 269-27 had a 20.3-mm-long reduced section, while specimens 269-4 and 269-8 had 10.1-mm-long reduced sections. Only specimen 269-27 penetrated substantially into the mandrel gap,

[11]Nikon Measurescope — Nippon Kogaku KK and Ehrenreich Photo-Optical Industries Electromike.

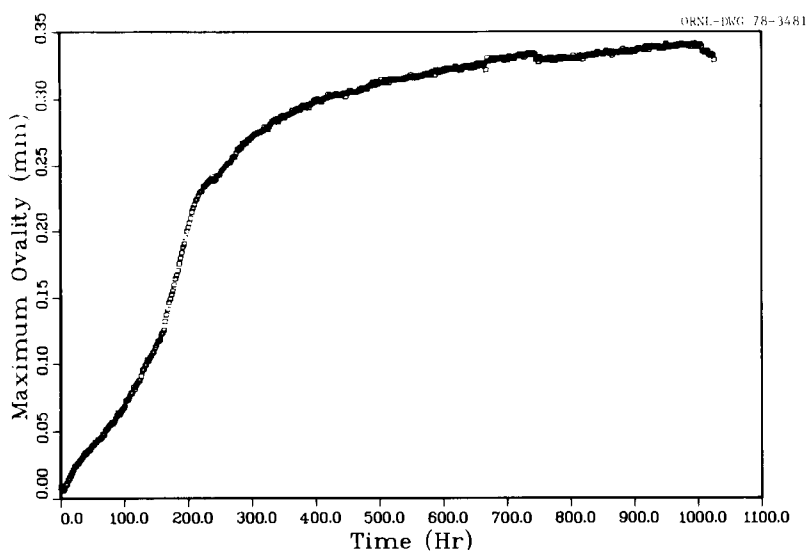

Fig. 20. Maximum measured Ovality in Test 269-4 (Diametrally Opposed, Orthogonal Pairs of Probes) as a Function of Time. Slope changes, particularly at approximately 230 hr, are caused by the maximum ovality shifting from one set of probes to another.

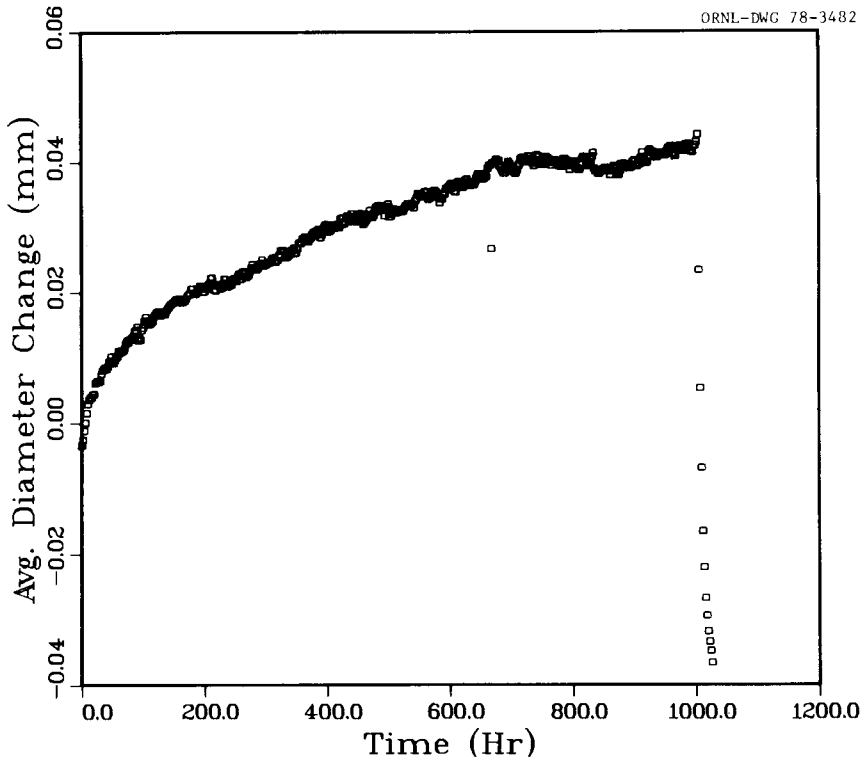

Fig. 21. Average Diameter Change as a Function of Time in Test 269-4. Note that scale is in terms of lift-off at the probe-coil assemblies. Therefore, a *positive* number indicates a diameter *decrease*.

but we estimate that all three center sections deformed freely. Tube 269, from which the test specimens were taken, had an average wall thickness variation of 0.025 mm (0.0010 in.) and it can be seen in Fig. 22 that the center section wall thicknesses vary approximately this much. The average wall thickness has, however, increased during creepdown. These results can be interpreted as uniform plane strain, in which the wall thickens uniformly as the circumference decreases, while the wall thickness variation is maintained.

The cross sections taken from the mandrel-supported part of the specimens behaved quite differently. Specimen 269-27 differed most markedly. This specimen was subjected to the higher test pressure for the longer times. Post-test examination of the section showed that the specimen had been supported by the mandrel over approximately 270° of the circumference. This had resulted in the formation of a single lobe, and it was in this portion that a large amount of wall thickening had taken place. Measurements showed an increase of 0.117 mm (0.0046 in.) at the point of the lobe over the average wall thickness.

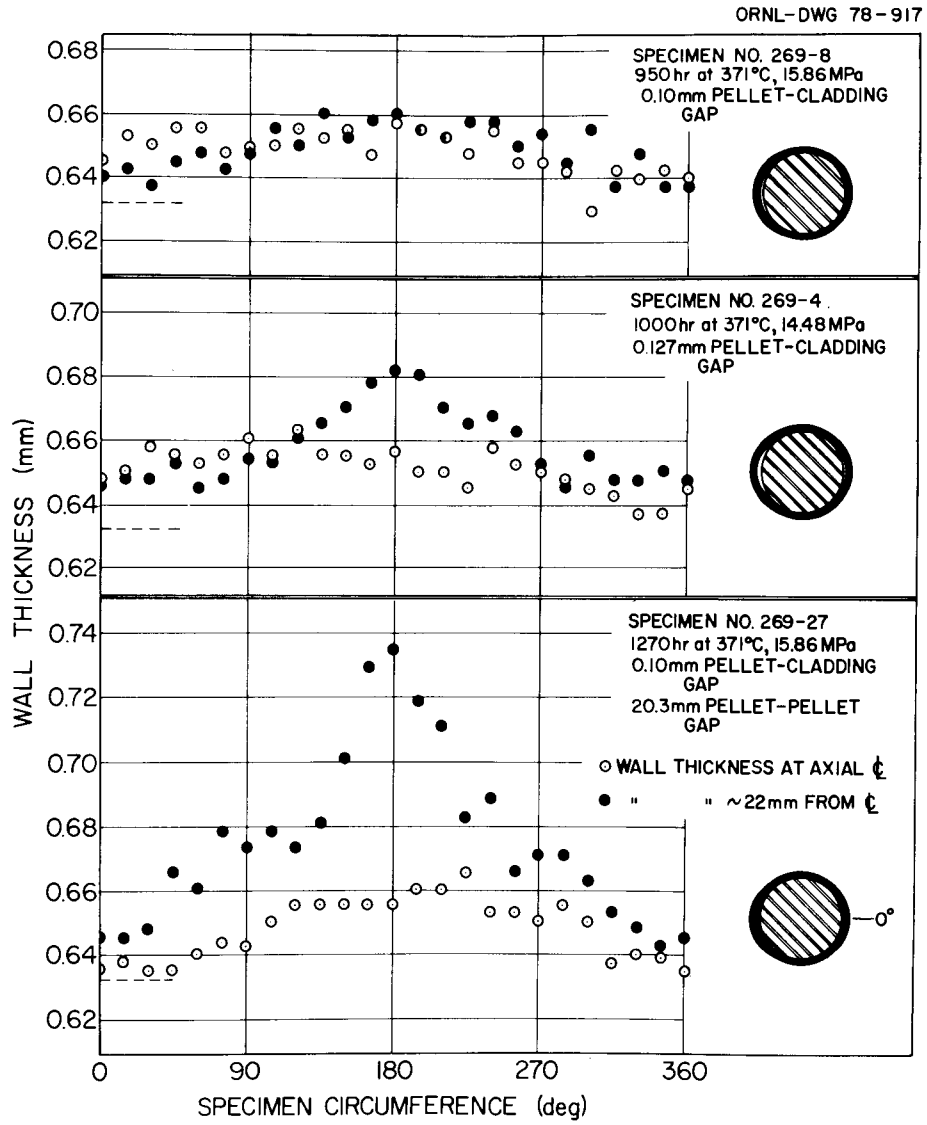

Fig. 22. Wall Thicknesses as a Function of Circumferential Position at Two Axial Locations — at the Axial Centerline and at a Position Supported by the Mandrel.

This result is interpreted in the following manner. In the early part of the test, before mandrel contact, the wall thickened relatively uniformly as the diameter (circumference) decreased. After the wall contacted the mandrel, more and more of the wall was supported by the mandrel, and deformation was confined to the remaining unsupported portions. Finally the only remaining unsupported portion, the single lobe, crept down and thickened.

The behavior of specimen 269-4 was similar but less pronounced. It had a larger initial mandrel-cladding gap and formed two lobes. The larger lobe showed a thickness peak. Specimen 269-8 peaked very little, possibly because it was tested for 326 hr less than was specimen 269-27, albeit under identical conditions.

The foregoing results should be of great interest to modelers of cladding behavior because the strain appears to follow a relatively simple pattern, and the two deformation types (ovalization and diameter decrease) appear to be decoupled to a large extent. This should simplify the task of describing cladding behavior.

Radius measurements, made on the cross sections of the three long-time specimens at the same time as the wall thickness measurements, show the ovalities that occurred in the specimens. Figures 23 through 26 show the inner and outer diameters of the centerline sections and the mandrel-supported sections. Specimen 269-27 (see Figs. 23 and 24) shows the greatest ovality, as expected. However, examination of specimen 269-27 reveals a discrepancy between the maximum ovalities found by the

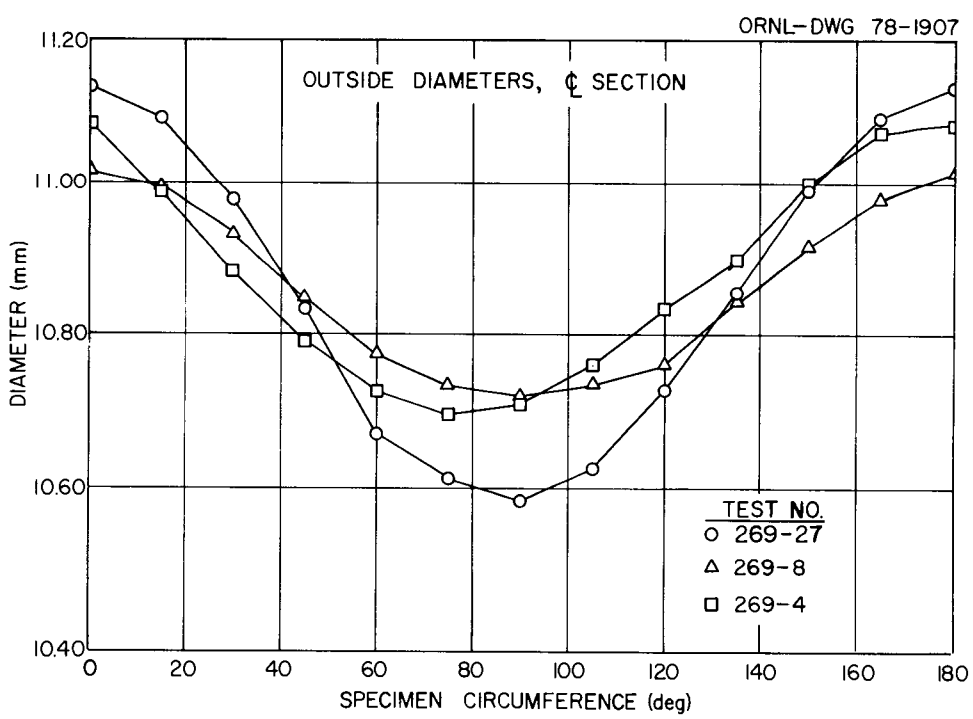

Fig. 23. Outside Diameters of Test Specimens Taken at the Axial Centerline.

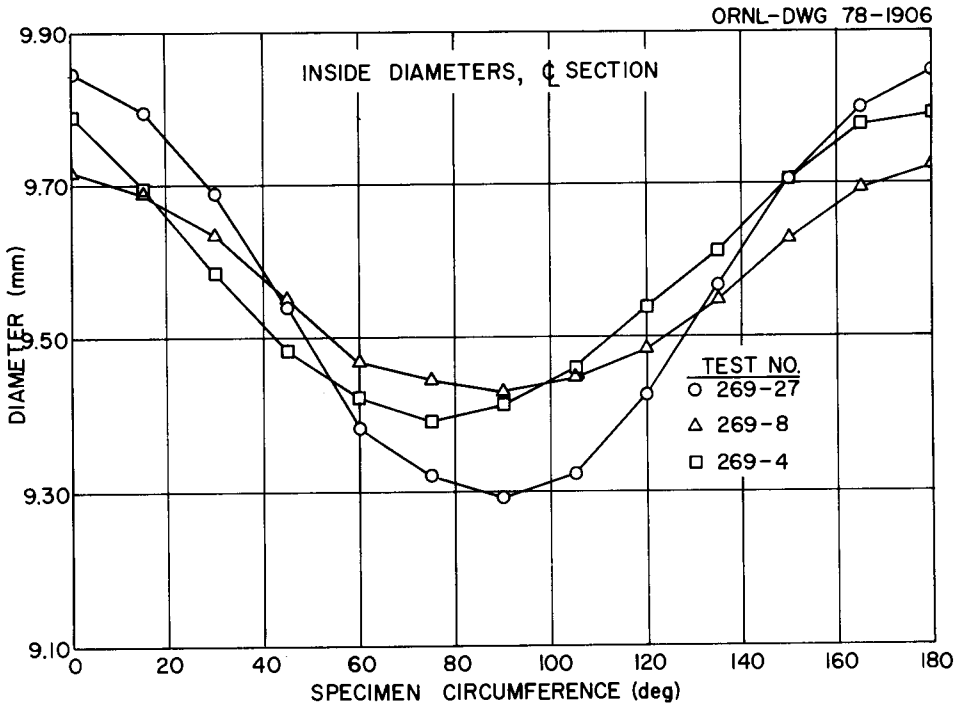

Fig. 24. Outside Diameters of Test Specimens Taken at the Axial Centerline.

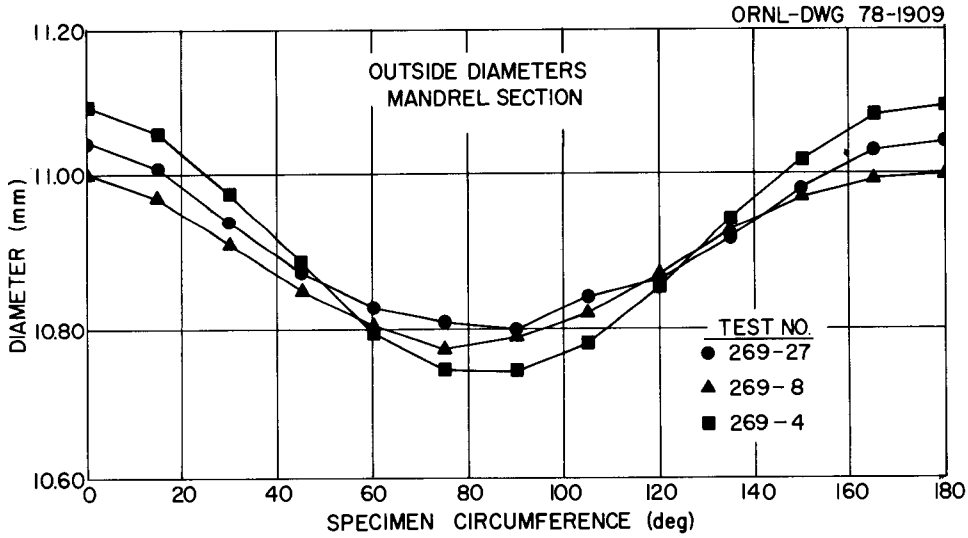

Fig. 25. Outside Diameters of Test Specimens Taken from Mandrel-Supported Cross Section.

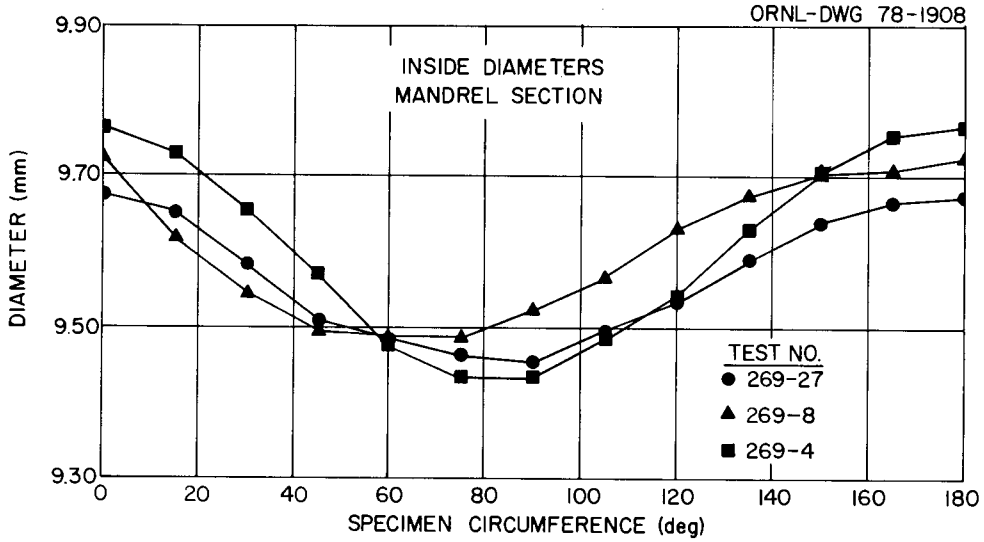

Fig. 26. Inside Diameters of Test Specimens Taken from Mandrel-Supported Cross Section.

two methods of measurement. The eddy-current data show a maximum difference in orthogonal diameters of 0.317 mm (0.0125 in.). On the other hand, measurements with the toolmakers microscope showed a maximum diameteral difference of 0.556 mm (0.0291 in.). This seemingly large discrepancy can easily be explained by examination of the analog model, which was pictured in Fig. 18. When the O-ring markers are set to correspond to the final set of test data (1270 hr) and the model is held for viewing parallel to the axis, the major diameter is found at a position midway between two sets of probe positions. This means that the eddy-current probes were removed circumferentially 20 to 25° from the actual maximum and minimum diameters of the test section. Reference to Fig. 23 showed that a circumferential movement of approximately 22 or 23° could easily decrease the major diameter and increase the minor diameter enough to reconcile the discrepancy.

Mathematical modeling

Although the foregoing descriptions of the creepdown deformations are graphic and provide a good qualitative feel for cladding shapes as a function of time, a more rigorous, quantitative description is necessary before strains and strain rates can be calculated from the data. To accomplish this requires mathematical modeling of the surface displacements.

The problem of describing the creepdown results in a form that can furnish information on strain rate and total strain is formidable. The movement of any point on the specimen surface is not necessarily a monotonic function of time after contact with the mandrel. Instead, the radial displacements can reverse direction and alter any symmetry the specimen might have had before contact. Such strain reversals imply stress reversals in the specimen wall, making the concept of creep rates somewhat cloudy.

Several paths can be taken to describe mathematically the displacements of the cladding. We have chosen the following:

$$x = [R_0 + \sum_{mn}\sum(\delta^1_{mn} \cos m\theta \cos \frac{n\pi z}{L} + \delta^2_{mn} \cos m\theta \sin \frac{n\pi z}{L}$$

$$+ \delta^3_{mn} \sin m\theta \cos \frac{n\pi z}{L} + \delta^4_{mn} \sin m\theta \sin \frac{n\pi z}{L})]\cos \theta \ ,$$

$$y = [R_0 + \sum_{mn}\sum(\delta^1_{mn} \cos m\theta \cos \frac{n\pi z}{L} + \delta^2_{mn} \cos m\theta \sin \frac{n\pi z}{L} \tag{1}$$

$$+ \delta^3_{mn} \sin m\theta \cos \frac{n\pi z}{L} + \delta^4_{mn} \sin m\theta \sin \frac{n\pi z}{L})]\sin \theta \ ,$$

and $z = z$

where

R_0 = initial radius of specimen,

$R = R_0 + \Sigma\Sigma\ (\quad)$ = radius of deformed specimen,

δ^i_{mn} = coefficients of equation,

L = constant related to periodicity of deformation,

θ = angle between surface point and reference plane (see Fig. 27).

These equations define a cylindrical surface with the z direction as the axis. The coordinate system is shown in Fig. 27.

Equation (1) can be used to model the shape of the specimen at any time for which a data set exists. In other words, a set of 20 isochronal displacement points, taken in conjunction with the starting specimen shape,

ORNL-DWG 78-2636

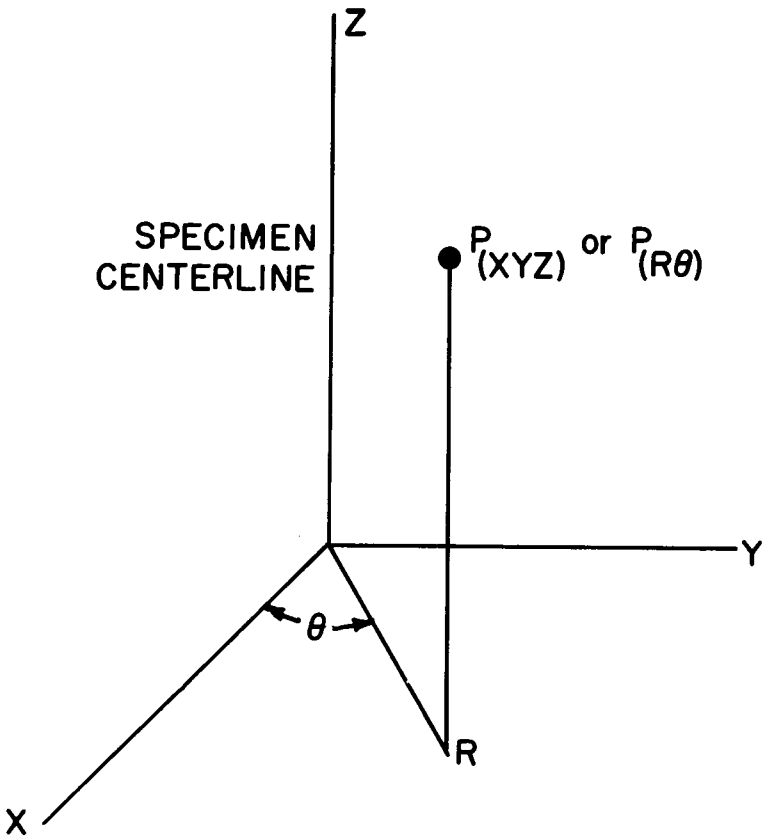

Fig. 27. Coordinate System for Modeling the Surface of Specimen.

can be represented by this model. The major drawback of this model is that it does not show the history of the shape changes in the specimen. There is no way to know the sequence of such changes and therefore the strain sequences within the wall as a function of time.

A second method for representing shape changes involves modeling the individual displacement curves for the probes as a function of time. The curves shown in Figs. 3 through 17 could be represented mathematically as functions of time. The substitution of a value for time into 20 separate equations would generate 20 separate surface displacements. These would be, however, only a little more useful than reading the actual values of the test data from a listing.

A third and more comprehensive mathematical method for representing surface displacements involves the modeling of the surface itself as a

function of time. Each long-time test comprises from 10,000 to 13,000 data points (20 points each at 2-hr intervals). Theoretically all these data could be used to model shape changes during the entire time period of each test.

The form of Eq. (1) is a representation of the deformed surface by double Fourier series. A limited number of terms can be used to approximate the geometry without a loss of generality. For a given probe geometry (probes arranged in a specific pattern around the specimen) and for specific sets of values of m and n, the trigonometric terms approximate the trend of the shape, whereas the δ^{i}_{mn} coefficients determine the amplitudes of those surface variations. Now, for the cases where mandrel contact has not been reached, all the data show monotonic behavior. It should be possible to model the surface by a simultaneous fit of an equation such as Eq. (1) to all the data up to the time of mandrel contact. The major difference would be that the δ^{i}_{mn} coefficients would be modeled as functions of time. This means that the general shape of the surface would be fixed, but the amplitudes of the displacements (relative to the original specimen shape) would vary with time. Such a model would provide the means for specifying specimen strain patterns with time and, therefore, the capability for determining strain rates of points within the cladding wall. It is precisely those strain rates — as a function of temperature, stress state, and ultimately neutron flux — that are needed by modelers of cladding behavior. Further creepdown testing will likely reveal a close correlation between original specimen geometry — such as ripples, wall thickness variations, and initial ovality — and the specimen shape changes. Those shape changes will depend directly, however, upon the stress states throughout the wall and on the variation of those states with time. Future reports will explore such mathematical modeling studies.

A given specimen of Zircaloy fuel cladding subjected to test temperatures and pressures will certainly exhibit a different creepdown strain pattern from that exhibited by any other specimen under similar conditions. The initial geometrical differences discussed above account for this difference. Once again, however, the relationship between strain rate and stress state should be amenable to correlation.

FUTURE WORK

The results presented and discussed in this report have opened up several paths for future investigation of the creepdown phenomenon that have very important implications to both modelers and other experimenters.

One of the most gratifying discoveries in this study was the excellent quality of the surface displacement measurements made by the eddy-current system. This measuring capability, in conjunction with the criteria of data applicability discussed earlier (p. 5), provides an incentive to attempt studies that would be difficult, if not impossible, with other measurement methods. These studies, and their rationale, will be discussed in the following sections.

Short-Term Tests

The subject of cladding creep is, as stated earlier, quite complicated. Part of the complexity is due to changes in geometrical boundary conditions during the creepdown test itself. The most obvious of these changes occurs when the cladding contacts the mandrel. Then the previously unsupported specimen begins to be supported at various points by the mandrel, and the stress and strain patterns change. Systematic testing should be able to define the strain patterns of specimens (as a function of external pressure and temperature) up to the time of mandrel contact — before the patterns are forced to change. A series of short-time tests are proposed at various external pressures, at constant temperature, and with various pellet-cladding gaps. These tests will be run for 100 to 500 hr and should provide a consistent set of specimen behavior patterns. In addition to the surface displacement measurement, we intend to provide a grid over the test section of each specimen to assist in interpreting the strain patterns. These tests should provide the following quantitative information:

1. time to first mandrel contact,
2. surface displacements under free creepdown conditions,
3. shape change pattern information.

The data from these tests are expected to vary in a definite manner with pressure and temperature, with the displacement probe outputs varying

monotonically. Such information should allow data for relatively severe test conditions to be extrapolated to the less severe pressure of normal reactor operation.

Long-Term Tests

Specimen behavior following initial mandrel contact is much more complicated than the free creepdown that takes place before such contact. Our initial tests have shown that local specimen wall thickening contributes to a large extent to the creepdown that takes place after contact. The plane-strain condition that seems to exist after contact may allow the sequence of creepdown to be interpreted from metallographic examination or from nondestructive eddy-current wall thickness measurements taken from specimens after testing. Indications are that the portions of the specimen wall that contact the mandrel cease to deform — that is, there is no further circumferential strain and, therefore, no further wall strain. Substantial wall thickening occurred (in Fig. 22, for Test 269-27) in the unsupported lobe that remained after most of the specimen inner circumference was in contact with the mandrel.

Further long-term tests will examine the relationships among wall thickening, pellet-cladding (mandrel-specimen) gap, and contact area.

CONCLUSIONS

This study has shown, on the basis of the initial creepdown tests reported herein, that the eddy-current surface displacement measurement system developed for this program is capable of exceptionally high accuracy and precision.

We have inferred by means of very accurate wall thickness measurements of tubular Zircaloy creepdown specimens that the plastic creep strains may be less complex than previously expected. Conservation of volume demands that any diametral (circumferential) strain be accommodated by corresponding axial and/or wall thickness strain. The only alternative would be for the tube wall to buckle and collapse. We used internal mandrels to

simulate fuel pellets and found that the 0.10 to 0.12-mm radial mandrel-to-cladding gap, typical of the pellet-to-cladding gap found in real fuel rods, prevented gross collapse. Whereas the unsupported cladding (no mandrel contact) undergoes diametral strain and uniform wall thickening, once the cladding contacts the mandrel the uniformity of the strain lessens. As creepdown progresses and more and more of the cladding is in close contact with the mandrel and supported by it, the remaining material forms one or more lobes. These unsupported portions continue to creep.

The important discovery is that the lobe seems to deform not by buckling or collapsing but by a plane-strain creep process involving tangential compressive and radial tensile strains. Although understanding and modeling creepdown behavior is still difficult, it now appears to be much less formidable than was previously thought. The information obtained in these tests has shown several significant areas for future experimentation in order to confirm and quantify the results of the initial tests.

ACKNOWLEDGMENTS

The author wishes to thank T. D. Owings for preparing and conducting the tests, C. V. Dodd and L. D. Chitwood for their continuing aid with the eddy-current instrumentation, B.L.P. Booker for the computer graphics, K. C. Liu and R. O. Williams for reviewing the manuscript. The author also wishes to thank Sigfred Peterson and Nancy Richards for editing and Kathryn A. Witherspoon for preparing this report.

ORNL/NUREG/TM-181
Distribution
Category NRC-3

INTERNAL DISTRIBUTION

1–2. Central Research Library
3. Document Reference Section
4–8. Laboratory Records Department
9. Laboratory Records, ORNL RC
10. ORNL Patent Office
11. P. Angelini
12. R. L. Beatty
13. E. Bolling
14. C. R. Brinkman
15. R. H. Chapman
16. L. D. Chitwood
17. J. A. Conlin
18. W. B. Cottrell
19. M. H. Fontana
20. T. G. Godfrey
21. J. A. Horak
22. R. F. Hibbs
23–25. M. R. Hill
26–45. D. O. Hobson
46. C. T. Liu
47. R. E. MacPherson
48. R. W. McClung
49. R. L. Moore
50. F. R. Mynatt
51. A. R. Olsen
52. T. D. Owings
53. R. E. Pawel
54. H. Postma
55. J. E. Selle
56. G. M. Slaughter
57. J. O. Stiegler
58. D. H. Thomas
59. K. R. Thoms
60. D. B. Trauger
61. M. H. Yoo

EXTERNAL DISTRIBUTION

62–69. Division of Reactor Safety Research, Nuclear Regulatory Commissio
Washington, DC 20545

70–72. ECN — Petten Research Center, Westerduinweg 3, Petten (NH), The Netherlands

G. W. Muysken
R. J. Swanenburg de Veye
Th. van der Kaa
N. van der Kleij

73–74. PNS — Leitung, Kernforschungzentrum Karlsruhe, Postfach 3640, 75 Karlsruhe, W. Germany

M. Fischer

75–77. Electric Power Research Institute, 3412 Hillview Ave., P.O. Box 10412, Palo Alto, CA 94303

M. Levenson (1)
W. Loewenstein (2)

78–79. Department of Energy Oak Ridge Operations Office, P.O. Box E, Oak Ridge, TN 37830

Director
Research and Technical Support Division

80–396. Given distribution as shown in Distribution Category NRC-3 (25 copies — NTIS)